

Supplemental information

**A living biobank of patient-derived ductal
carcinoma *in situ* mouse-intraductal xenografts
identifies risk factors for invasive progression**

Stefan J. Hutten, Roebi de Bruijn, Catrin Lutz, Madelon Badoux, Timo Eijkman, Xue Chao, Marta Ciwinska, Michael Sheinman, Hendrik Messal, Andrea Herencia-Ropero, Petra Kristel, Lennart Mulder, Rens van der Waal, Joyce Sanders, Mathilde M. Almekinders, Alba Llop-Guevara, Helen R. Davies, Matthijs J. van Haren, Nathaniel I. Martin, Fariba Behbod, Serena Nik-Zainal, Violeta Serra, Jacco van Rheenen, Esther H. Lips, Lodewyk F.A. Wessels, Grand Challenge PRECISION Consortium, Jelle Wesseling, Colinda L.G.J. Scheele, and Jos Jonkers

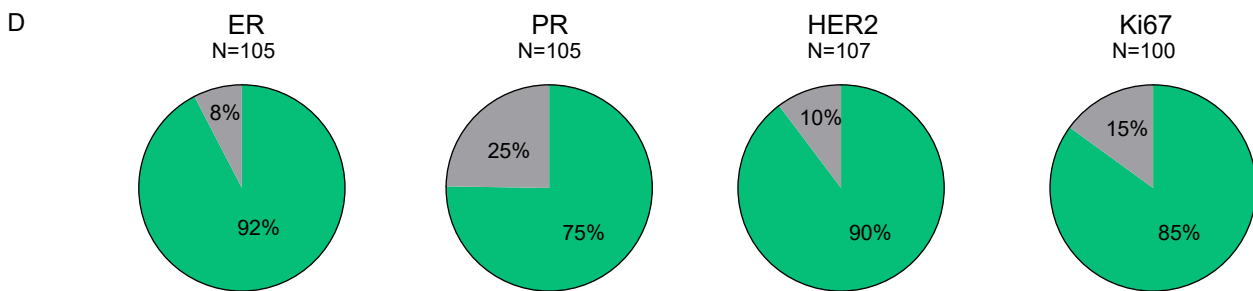
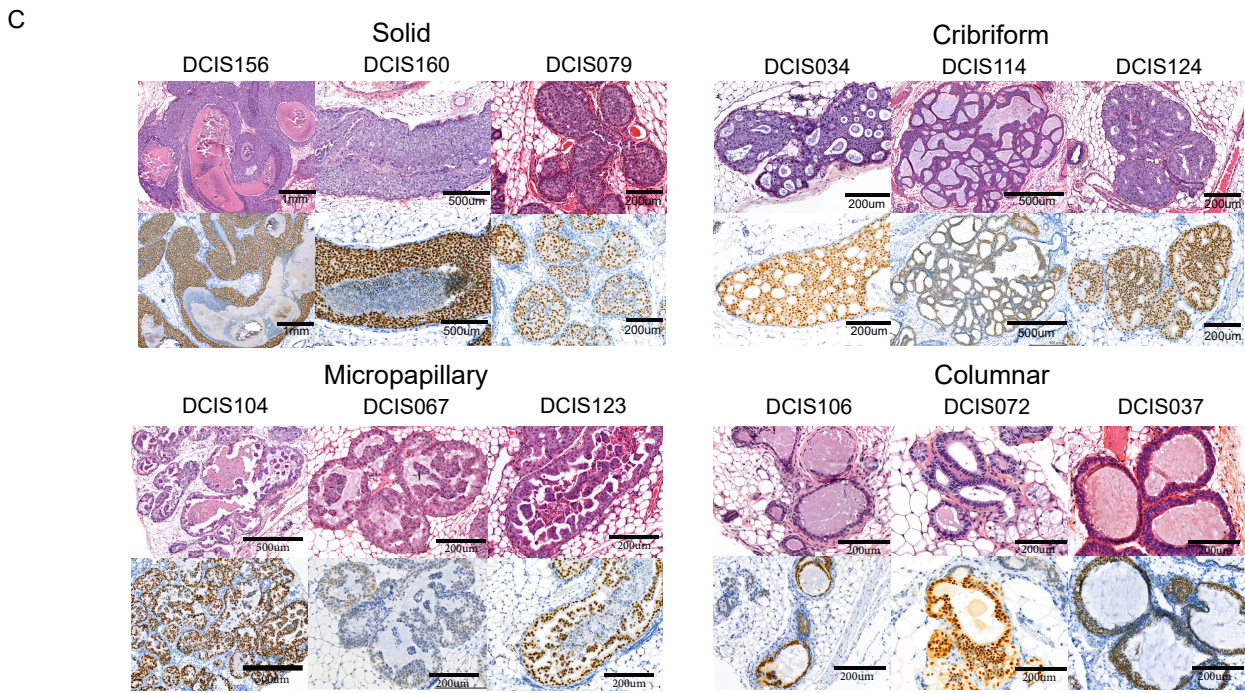
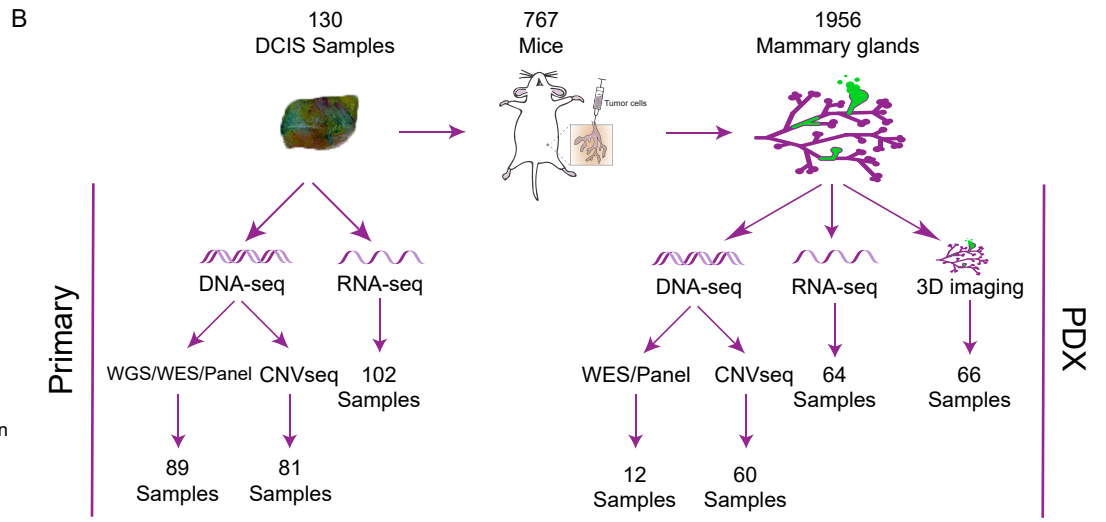
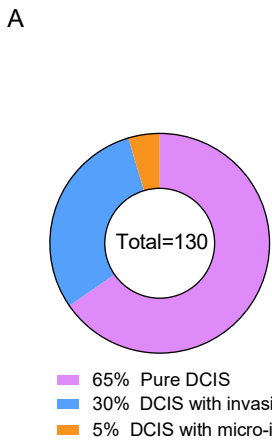
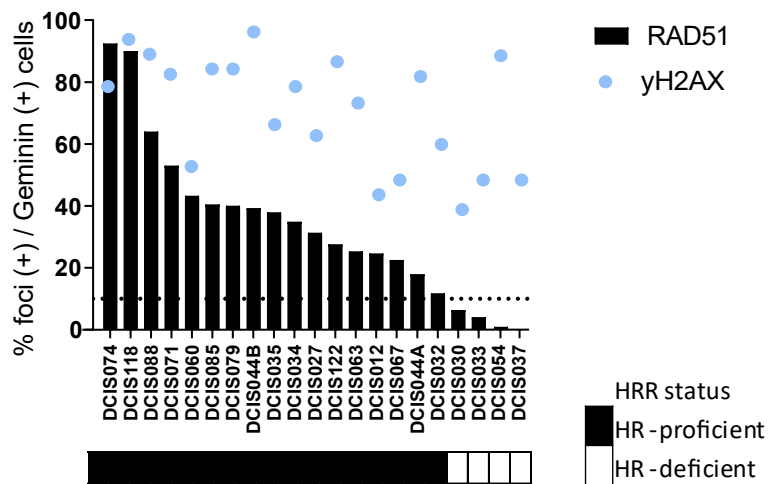


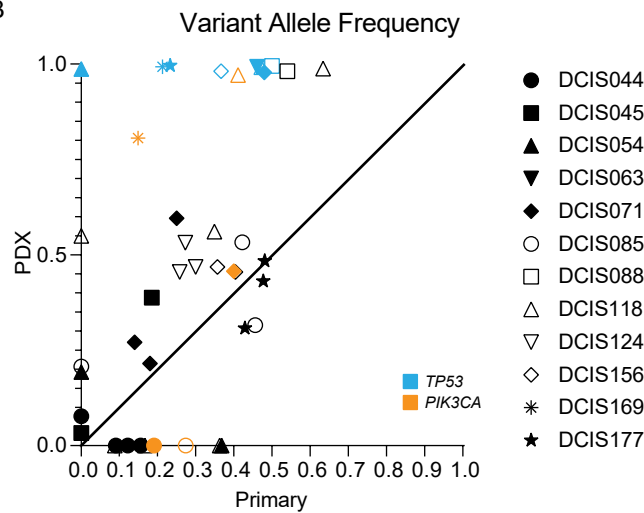
Figure S1. A comprehensive collection of 130 DCIS-MIND models, related to figure 1.

A) Pie chart of origin of DCIS with pure DCIS, DCIS with adjacent IBC or DCIS with micro-invasion. **B)** Schematic overview of the DCIS-MIND model collection and analyses performed on DCIS-MIND samples and primary DCIS lesions. **C)** Additional representative H&E (top) and human-specific Ku80 (bottom) images of DCIS-MIND models with a solid, cribriform, (micro-)papillary or columnar growth pattern. **D)** Pie charts of concordance between the primary DCIS lesion and matched DCIS-MIND lesion for ER, PR, HER2 and Ki67 respectively (green is concordant, grey is discordant). ER, PR and HER2 is concordant when both cases are positive ($\geq 10\%$ cells positive) or negative ($\leq 10\%$ cells positive), Ki67 is concordant when the percentage of positive cells is within 10% difference.

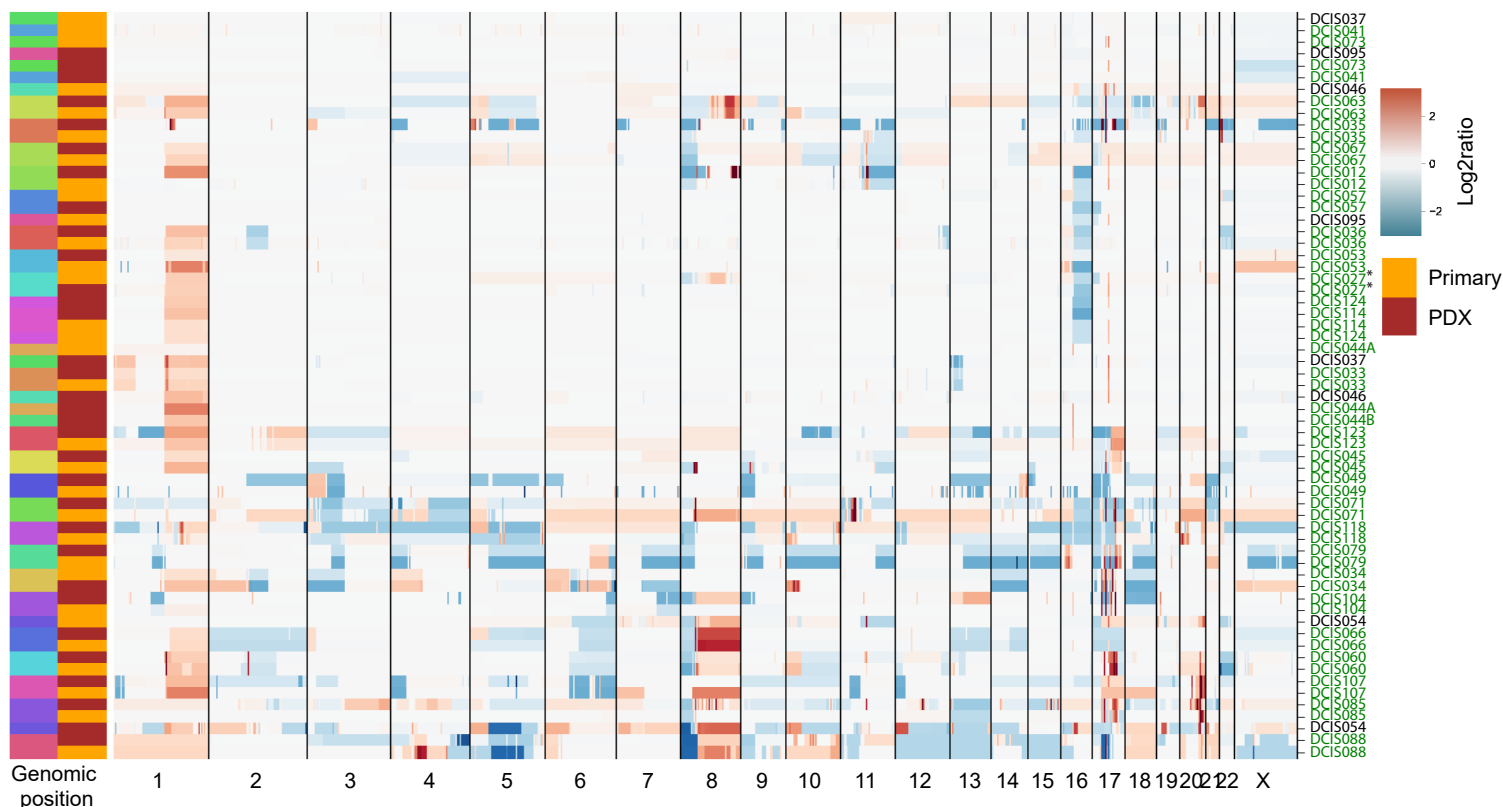
A



B



C



D

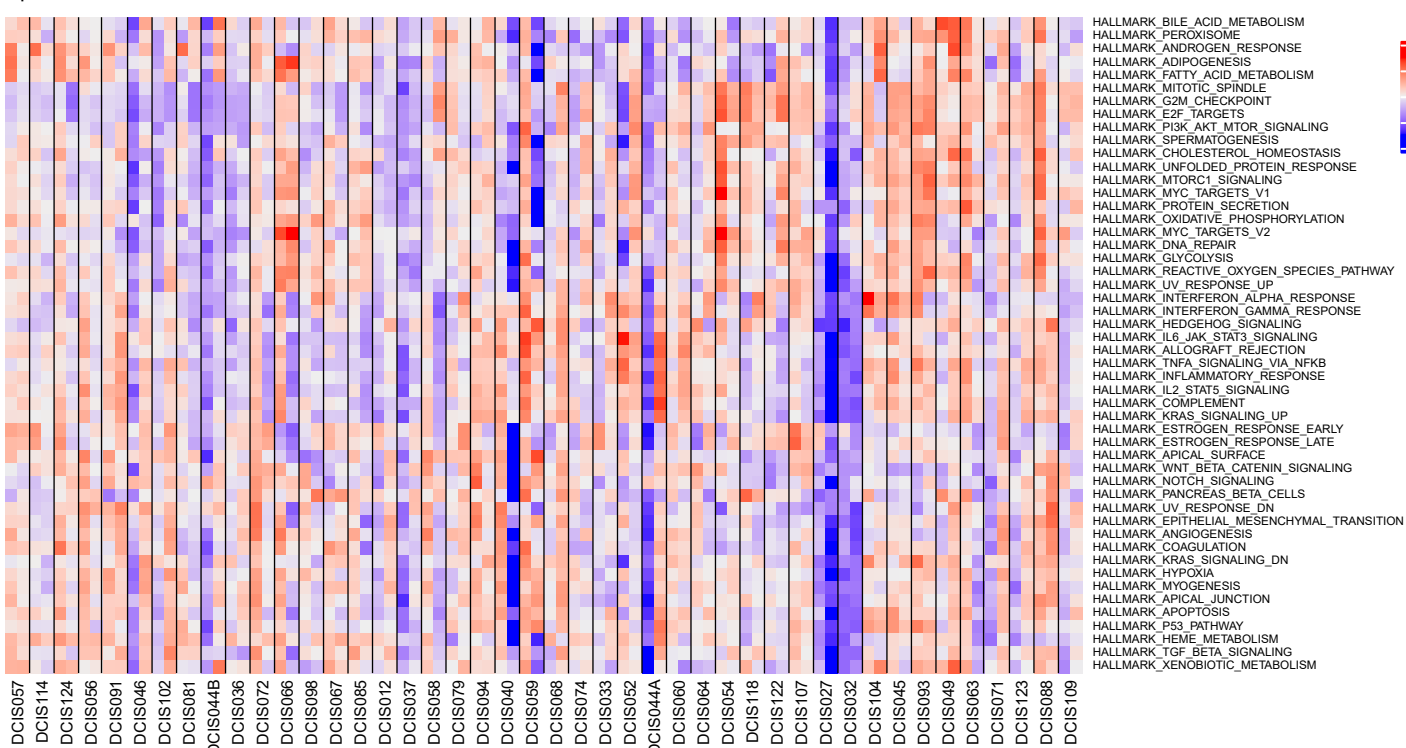
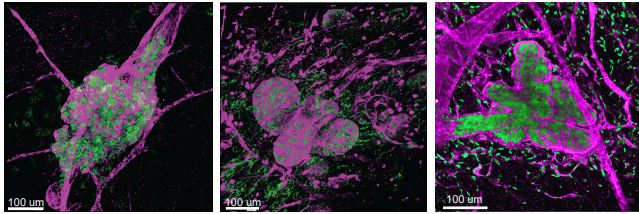


Figure S2. RAD51 assay and RNA expression profile correlation, related to figure 2

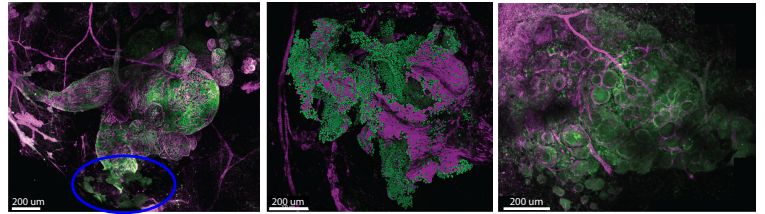
A) RAD51 score of a subset of DCIS-MIND models. Models are homologous recombination proficient (HR- proficient), when $\geq 10\%$ of cells have ≥ 5 RAD51 foci. **B)** Variant allele frequency (VAF) analyses comparing matched primary DCIS and DCIS-MIND samples, TP53 mutations are indicated in blue and PIK3CA mutations in orange. **C)** Unsupervised clustering of primary DCIS lesions and corresponding DCIS-MIND lesions, based on Copy number aberration (CNA), where blue indicates losses and red indicates gains. Matched primary/MIND models are color-coded and green model annotation indicates a high concordance in CNA. **D)** ssGSEA analyses performed on matched primary DCIS and DCIS-MIND samples and clustered together to show retained expression.

A

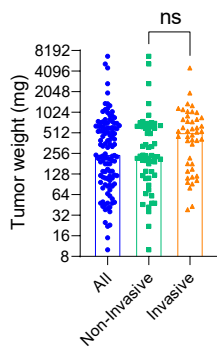
Non-invasive growth



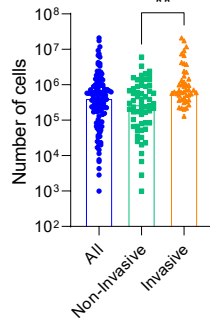
Invasive growth



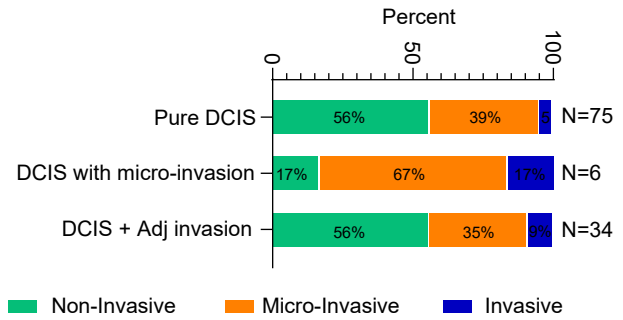
B



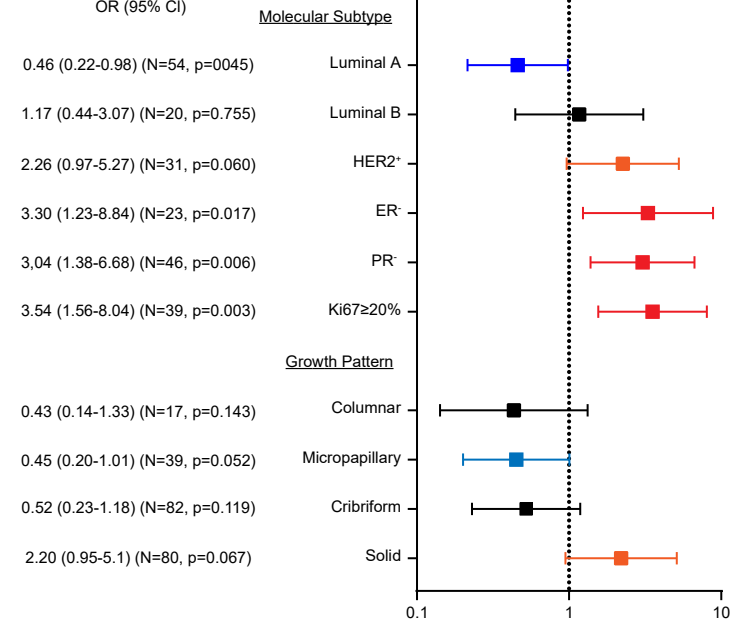
C



D



E

Univariate linear regression analyses
OR (95% CI)

F

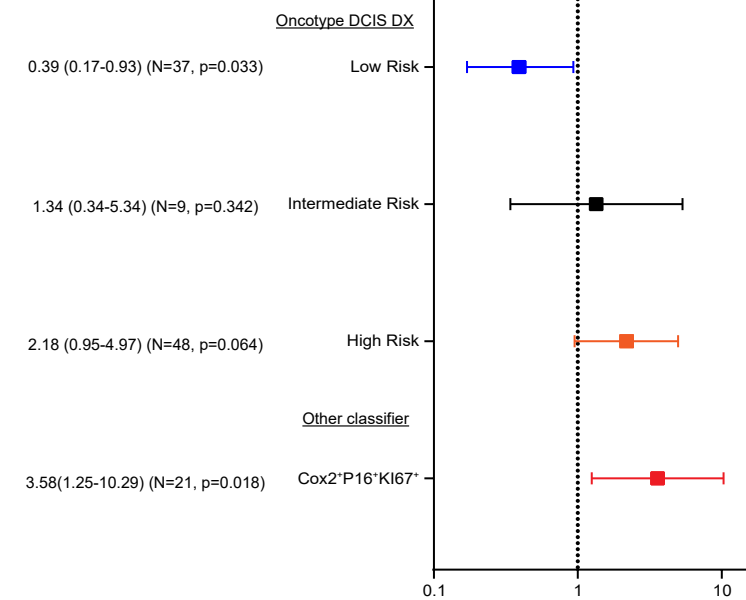
Univariate linear regression analyses
OR (95% CI)

Figure S3. Whole-mount images of non-invasive vs invasive growth and additional

parameters related to invasive progression, related to figure 3

A) Additional whole-mount images of non-invasive growth (left) and invasive growth (right).

Cells of human origin are marked with Ku80 (green), myoepithelial cells are marked with α SMA

(magenta). Blue circle indicates invasive cells. **B)** Boxplot of tumor weight of DCIS samples

received, divided by all, non-invasive and invasive DCIS-MIND models. Data are represented as

mean \pm SEM. Unpaired two-tailed Student's t test. ns, not significant. **C)** Bar plot of number of

cells obtained after processing of DCIS samples received, divided by all, non-invasive and

invasive DCIS-MIND models. Data are represented as mean \pm SEM. Unpaired two-tailed

Student's t test. $^{**}p < 0.01$. **D)** Diagram showing the distribution of non-invasive, micro-

invasive and invasive progression of DCIS-MIND models, comparing models originating from

pure DCIS, DCIS with micro-invasion and DCIS with adjacent invasion **E)** Odds ratio table

showing univariate risk scores for association between molecular subtype and growth pattern

parameters and invasive progression of DCIS in MIND-PDX models based on patient

characteristics. **F)** Odds ratio table showing univariate risk scores for the Oncotype DX DCIS- and

COX2⁺P16⁺Ki67⁺ classifier based on primary data.

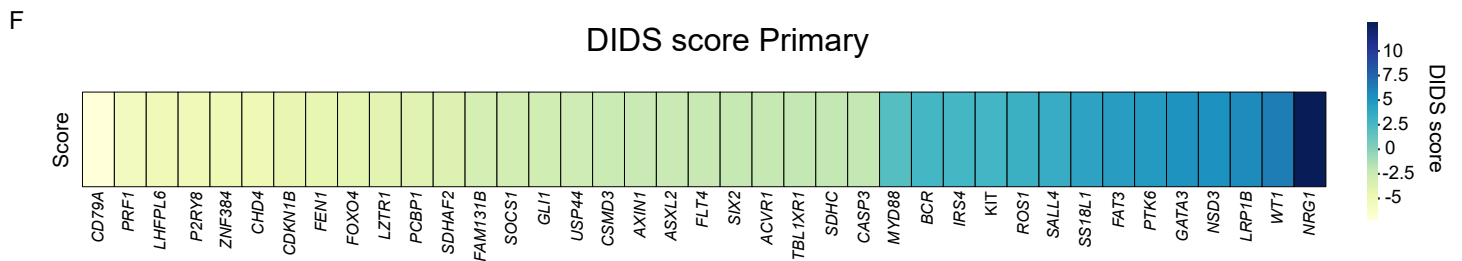
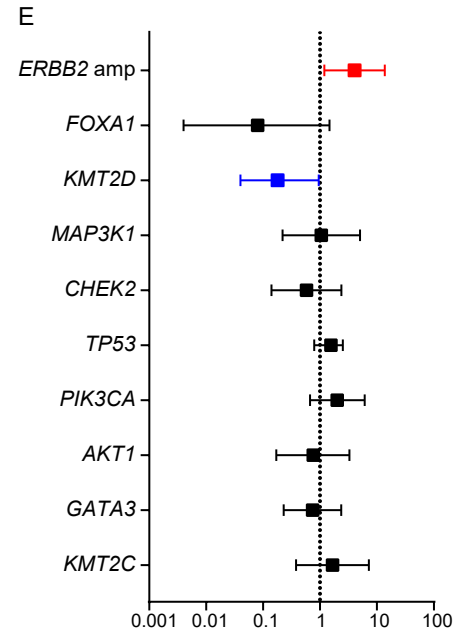
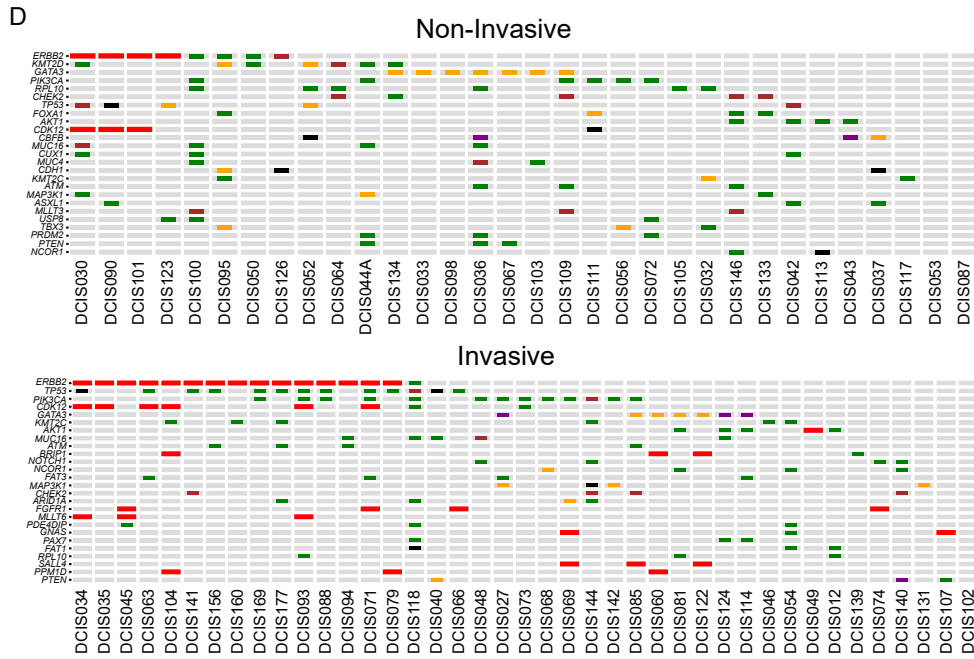
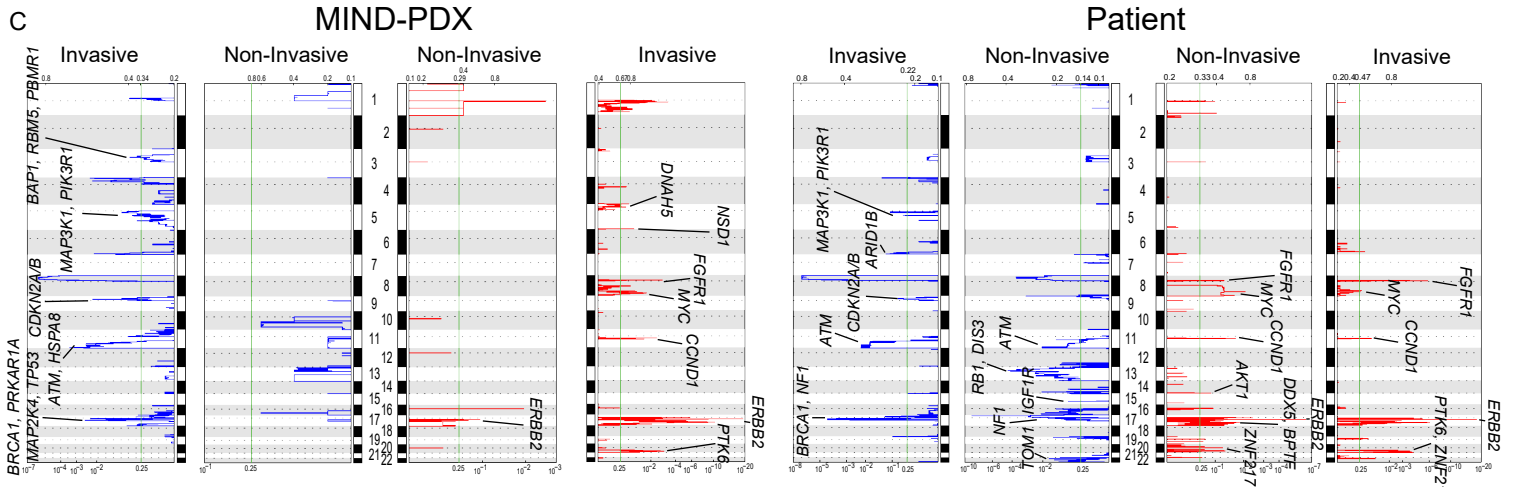
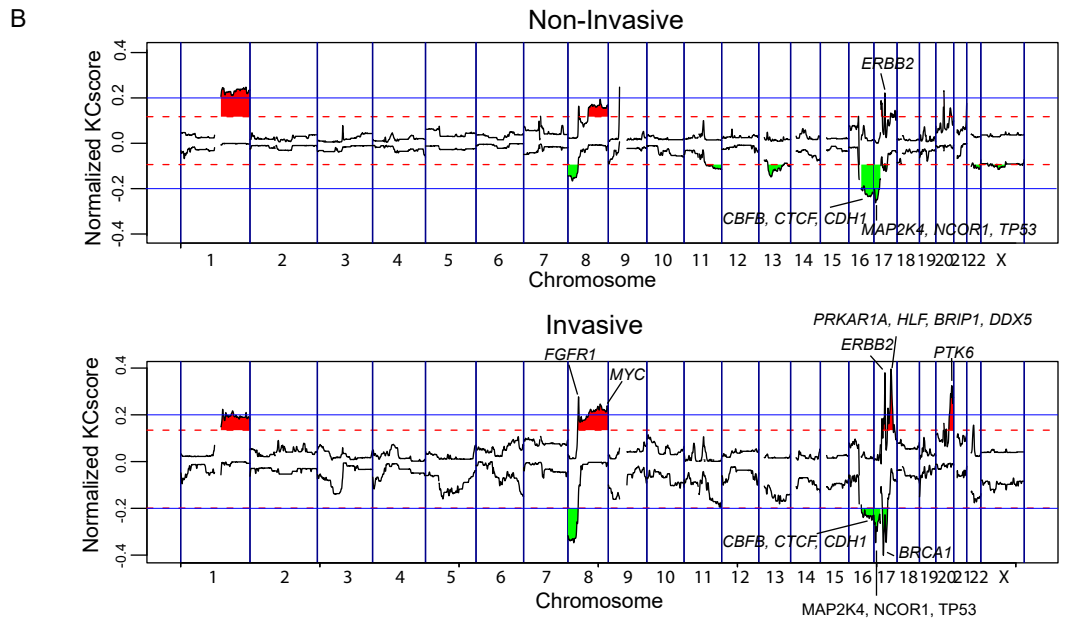
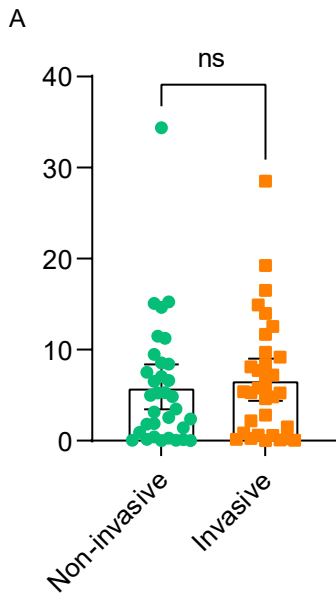


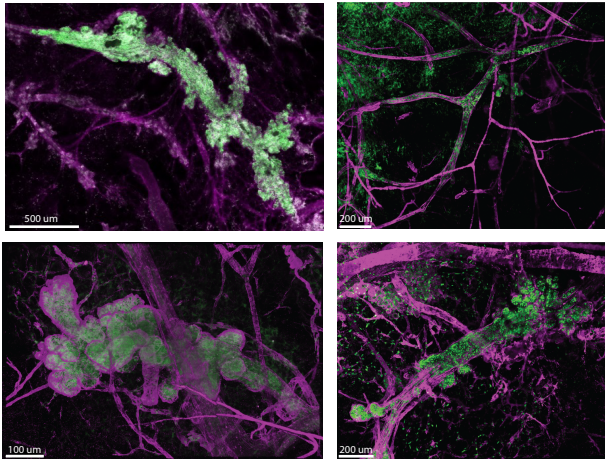
Figure S4. Comprehensive molecular analyses of primary DCIS for low-risk DCIS vs high-risk

DCIS and GISTIC2, related to figure 4

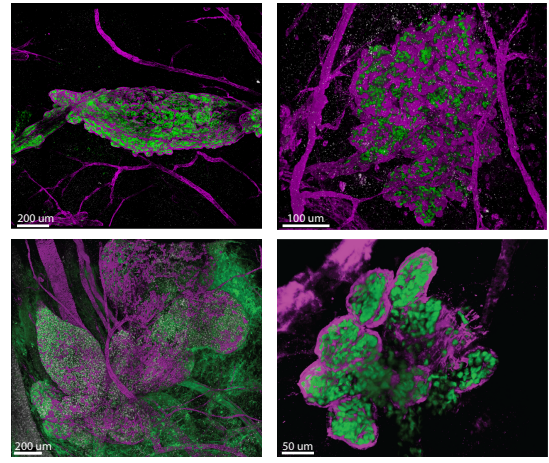
A) Scatter plot of percentage of genome with copy number alterations in matched primary DCIS lesions of DCIS-MIND models. Data are represented as mean \pm SEM. Unpaired two-tailed Student's t test. ns, not significant. **B)** KCSmart analysis of CNV-seq data of primary DCIS from non-invasive DCIS models (top panel) and invasive DCIS models (lower panel), showing recurrent DNA copy number losses and gains. Non-invasive DCIS models show recurrent 1q gains and 16q losses, whereas invasive DCIS models show recurrent amplifications of *FGFR1*, *MYC*, *CCND1*, *ERBB2* and *PTK6* as well as losses of *MAP3K1* and *CDKN2A/B*. Genes from our breast cancer gene panel were annotated. **C)** GISTIC2 analysis of CNV-seq data of DCIS-MIND models (left panels) and primary DCIS lesions (right panels) from non-invasive DCIS models and invasive DCIS models. Blue: deletion; Red: Gain, Genes from our breast cancer gene panel were annotated. **D)** Oncoprint showing the mutational landscape of the primary DCIS lesions corresponding to the non-invasive (Top) and invasive (Bottom) DCIS-MIND models, respectively, including amplifications, single-nucleotide variants and insertion-deletions (indels) for the top mutated genes. **E)** Odds ratio table showing risk scores for commonly mutated genes, indicating *ERBB2* amplifications and *KMT2D* mutations as significant odds ratio scores. **F)** Detection of Imbalanced Differential Signal (DIDS) scores for differentially expressed genes between primary DCIS lesions from non-invasive and invasive DCIS models.

A

Replacement growth

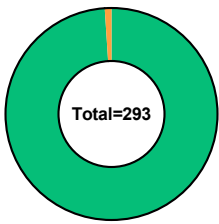


Expansive growth



B

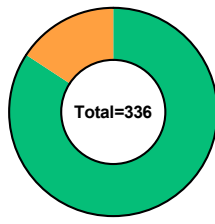
Replacement lesions



99% Non-Invasive
1% Invasive

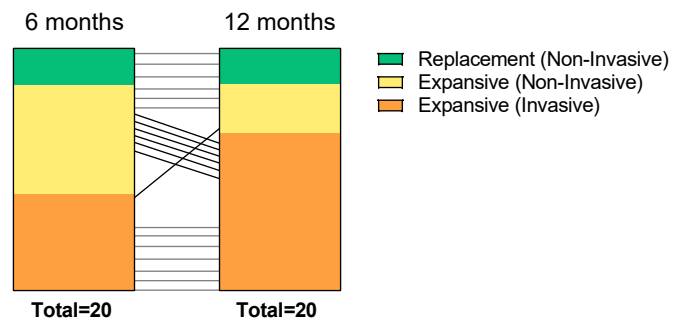
C

Expansive lesions

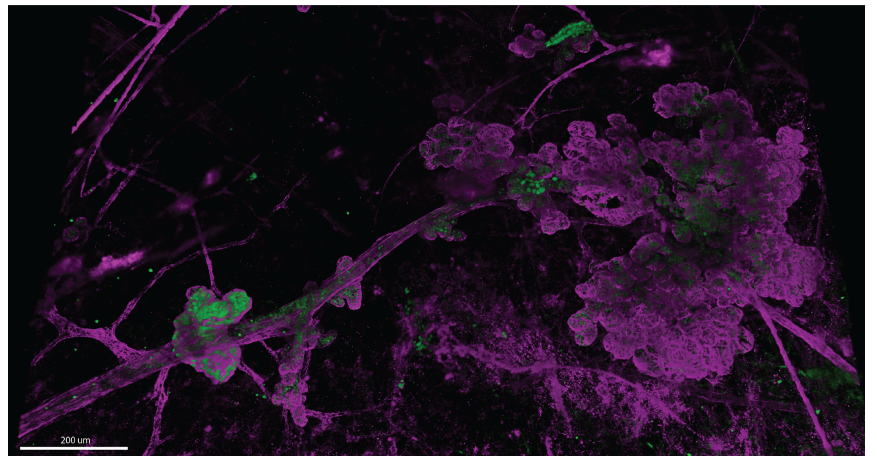
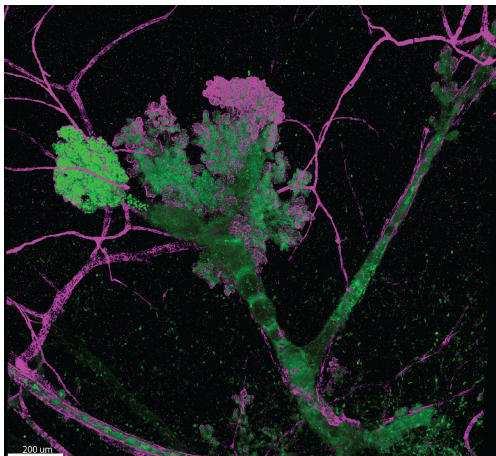


84% Non-Invasive
16% Invasive

D

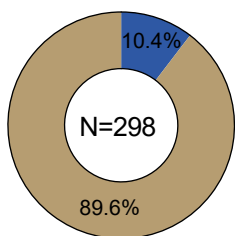


E



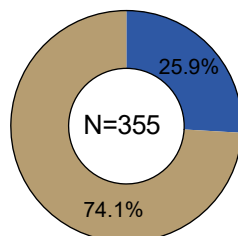
F

Replacement growth



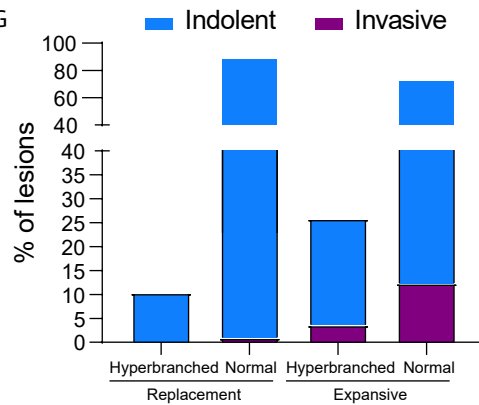
Hyperbranched

Expansive growth



Normal

G



H

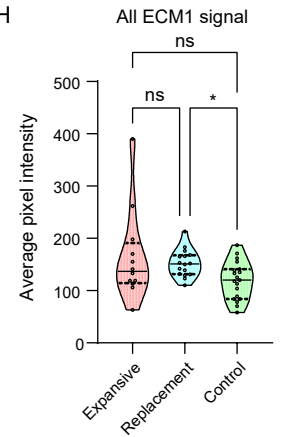


Figure S5. 3D growth pattern analyses and hyperbranching, related to figure 5

A) Examples of 3D whole-mount imaging of DCIS-MIND lesions, showing replacement growth (left panel) and expansive growth (right panel). Cells of human origin are marked with Ku80 (green), myoepithelial cells are marked with α SMA (magenta). **B)** Percentage of DCIS lesions showing invasion with replacement growth. **C)** Percentage of DCIS lesions showing invasion with expansive growth. **D)** Comparison of 3D growth pattern and invasion at an early- and late time point, 6 months and 12 months respectively. Grey line indicates concordance between early- and late time point, whereas a black line indicates a discordance between early- and late time point. **E)** Representative confocal whole-mount images of hyperbranching occurring around DCIS lesions. Cells of human origin are marked with Ku80 (green), myoepithelial cells are marked with α SMA (magenta) **F)** Percentage of replacement (left) and expansive (right) lesions with hyperbranching. **G)** Bar chart of percentage of DCIS lesions with invasive progression per 3D growth pattern, with or without hyperbranching. **H)** Quantification of total ECM1 expression in DCIS lesions for expansive or replacement growth, and normal mammary ducts. Lines indicate Q^1 , Median and Q^3 . Two-tailed Mann-Whitney test. * $p < 0.05$, ns, not significant.

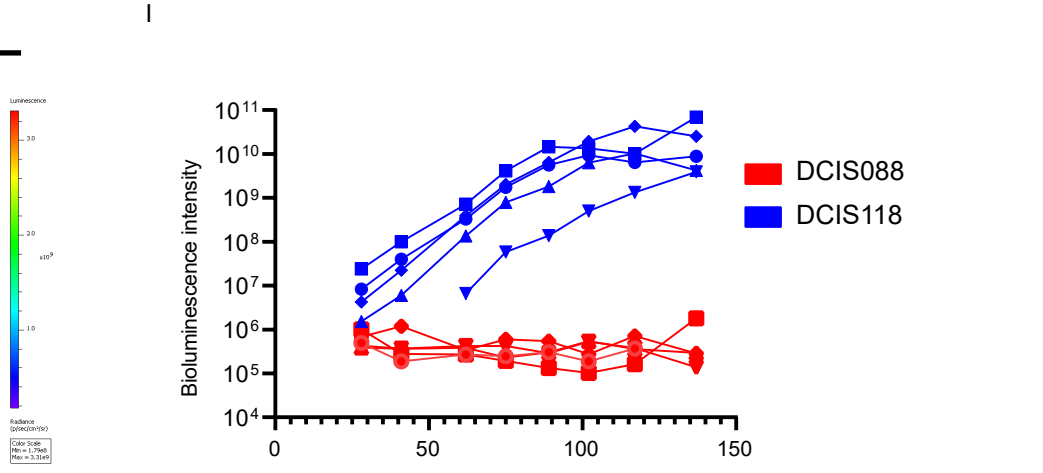
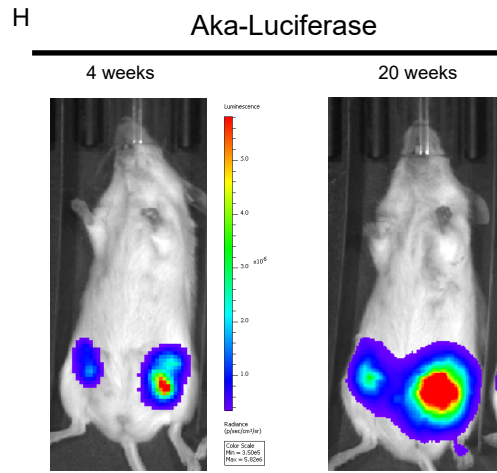
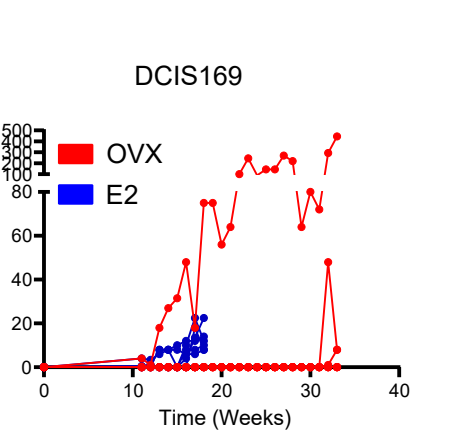
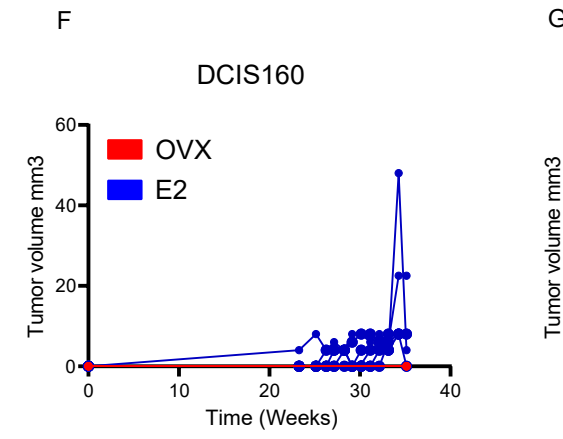
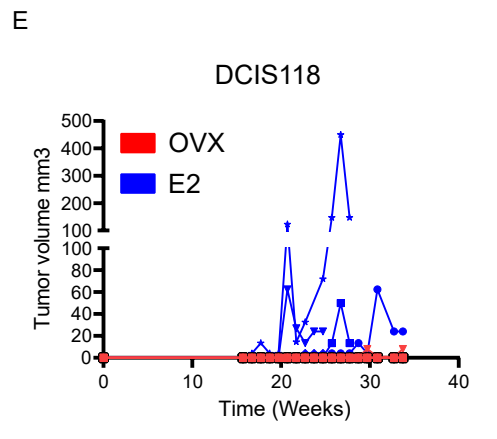
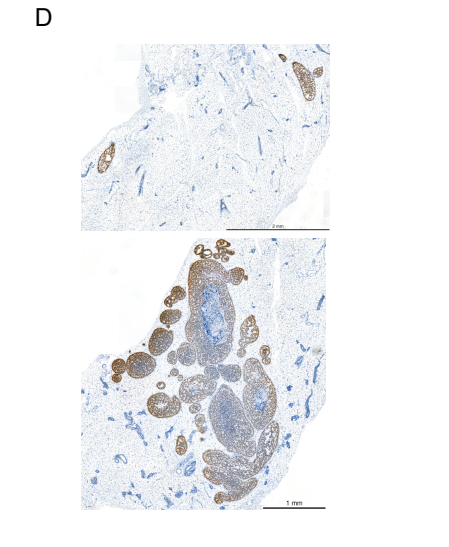
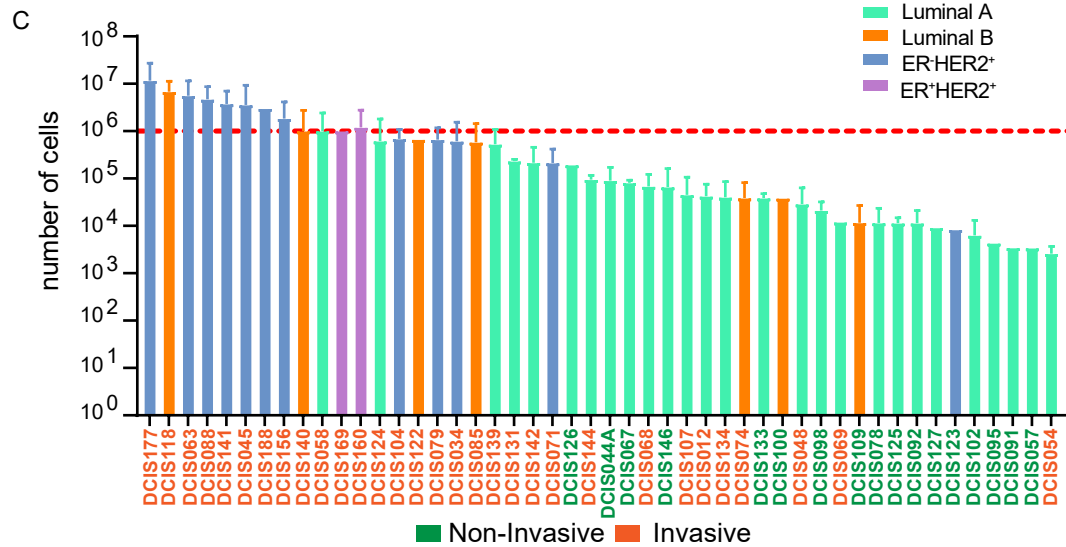
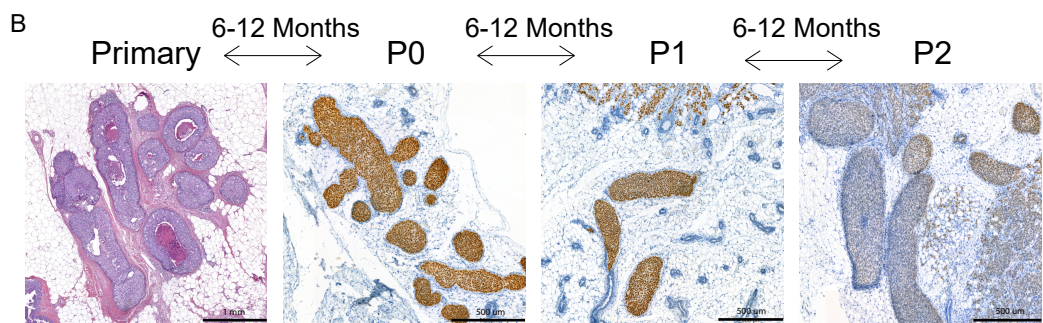
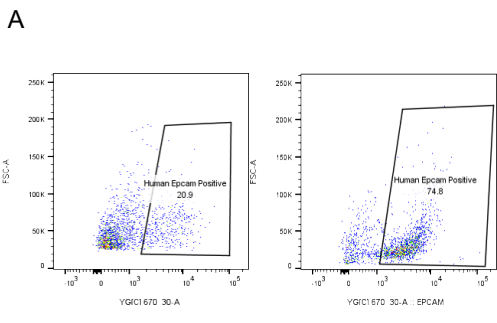


Figure S6. Sequential transplantation of DCIS and applications, related to figure S6

A) Representative FACS plot of human epithelial cells in a passaged sample marked with EpCAM, before (left) and after (right) magnetic bead sorting. **B)** Representative images of the growth pattern of DCIS118 as primary lesion (H&E), P0 (Ku80), P1 (Ku80) and P2 (Ku80). **C)** Distribution of the average number of tumor cells harvested from DCIS passages. Nineteen transplantable DCIS models yield more than 1,000,000 cells per passage and are therefore suitable for distribution to other labs. Data are represented as mean \pm SEM. **D)** Representative images of DCIS085 outgrowth (Ku80) in ovariectomized (OVX) mice (top) and in E2 supplemented mice (bottom) **E-G)** Growth curves of DCIS118 (**E**), DCIS160 (**F**) and DCIS169 (**G**) outgrowth in OVX mice and in E2-supplemented mice (E2 supplemented mice of DCIS169 had to be sacrificed at 18 weeks due to an infection). **H)** Representative images of bioluminescence of DCIS118 with Akaluciferase at 4 weeks (left) and 20 weeks (right) after injection. **I)** Bioluminescence intensity curves of DCIS118-Akaluciferase and DCIS088-Akaluciferase.

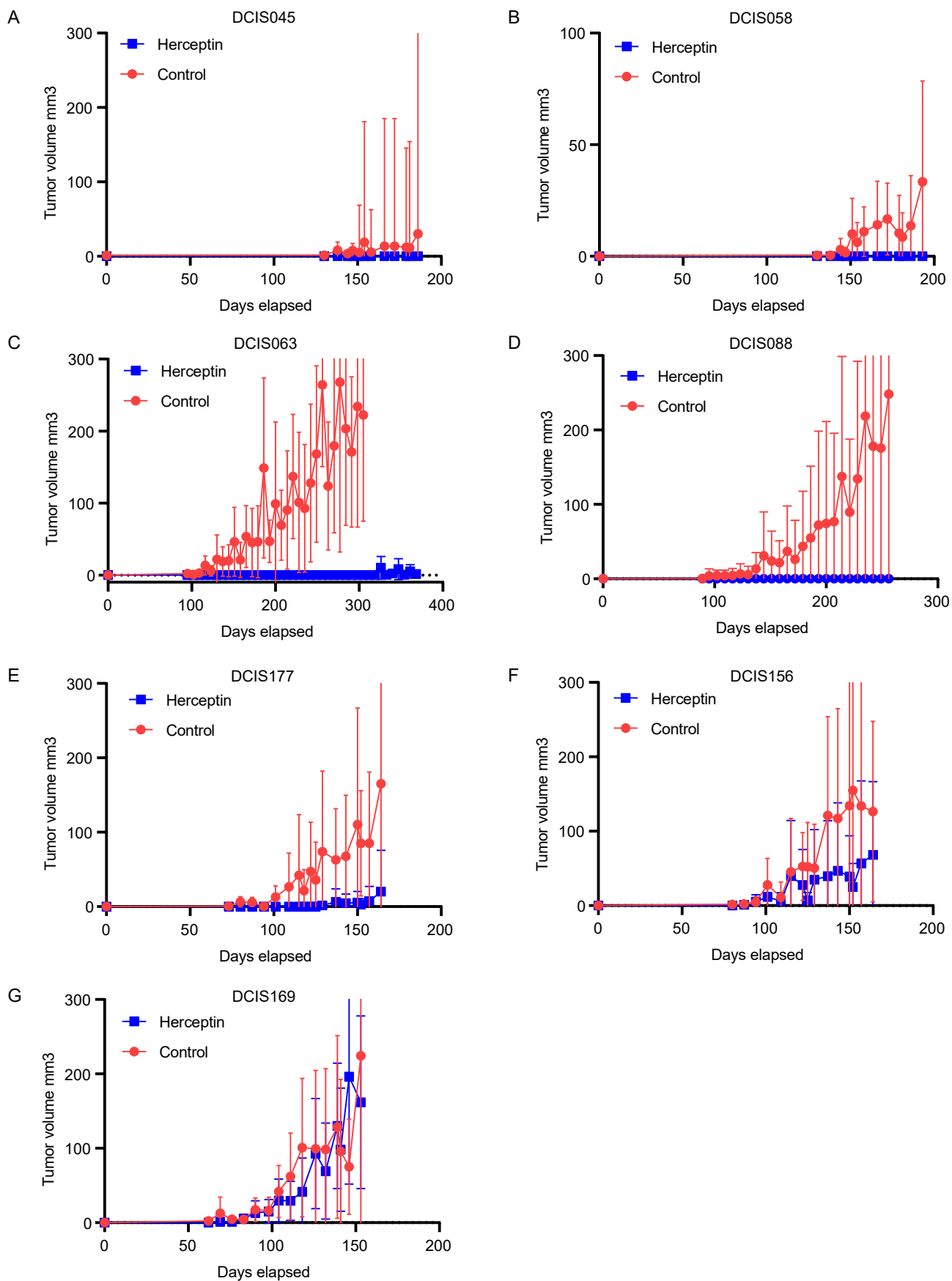


Figure S7. Altering HER2 expression changes growth kinetics of DCIS, related to figure S7

A-G) Growth curves of DCIS045 (**A**), DCIS058 (**B**), DCIS063 (**C**), DCIS088 (**D**), DCIS177 (**E**), DCIS156 (**F**), DCIS169 (**G**) with Herceptin treatment (10 mg/kg) or vehicle.